Preliminary Test Results on the New Electronic Readout of the YAP-(S)PET Small Animal Scanner

S. Chiozzi, A. Cotta Ramusino, C. Damiani, A. Del Guerra, *Senior Member, IEEE*, G. Di Domenico, R. Malaguti, E. Tonini, and G. Zavattini

***Abstract*—A small animal PET-SPECT scanner (YAP–(S)PET) prototype was built at the Physics Department of the University of Ferrara and is presently being used at the Nuclear Medicine Department for radiopharmaceutical studies on rats. The first YAP-(S)PET prototype shows very good performances, but needs some improvements before it can be used for intensive radiopharmaceutical research. The main problem of the actual prototype is its heavy electronics, based on NIM and CAMAC standard modules. For this reason a new, compact readout electronics was developed and tested. The results of a first series of tests made on the first prototype will be presented in this paper.**

I. Introduction

THE YAP-(S)PET scanner is a small animal positron emission tomograph recently built at Ferrara University. The scanner was in a second time adapted to also work as a single photon emission tomograph and it is presently being used for single photon emission tomography (SPET) at the Nuclear Medicine Department of the University of Ferrara. A complete set of studies and tests on the scanner performances have been published [1]. Preliminary studies on rats have been performed and reported [2]. The first results obtained with the scanner working as a single photon emission tomograph were recently published [3], [4]. The experimental results obtained with the YAP-(S)PET scanner suggested the further improvements in order to make the scanner easier to move and use by medical doctors and biology researchers. The main problem with the use of the first YAP-(S)PET prototype is the readout and data acquisition system, which is based on standard nuclear instruments methods (NIM) and computer aided measurement and control (CAMAC) modules and for this reason is heavy to transport and unfriendly to manage by non specialists. A new, compact, electronic readout was designed, realized and tested in collaboration with the Electronics Group of Ferrara Section of the National Institute of Nuclear Physics (INFN). The basic project and the first preliminary test measurements on the new YAP-(S)PET readout electronics are presented in this paper.

Manuscript received November 4, 2001; revised June 4, 2002.

S. Chiozzi, A. C. Ramusino, and R. Malaguti are with INFN Ferrara, via Paradiso 12, 44100 Ferrara, Italy (e-mail: cotta@fe.infn.it; chiozzi@fe.infn.it; malaguti@fe.infn.it).

C. Damiani, G. Di Domenico, E. Tonini and G. Zavattini are with the Department of Physics of the University of Ferrara, via Paradiso 12, 44100 Ferrara, Italy (e-mail: damiani@fe.infn.it; didomenico@fe.infn.it; zavattini@fe.infn.it).

A. Del Guerra is with the Department of Physics of the University of Pisa, p.zza Torricelli 2, 56100 Pisa, Italy (e-mail: delguerra@pi.infn.it).

Digital Object Identifier 10.1109/TNS.2002.803892

II. The New Electronic Read Out for the YAP-(S)PET Scanner

The YAP-(S)PET tomograph consists of two pairs of opposite detectors mounted on a rotating gantry. Each single detector is composed of a scintillator crystal matrix directly coupled to a Hamamatsu R2486-06 position sensitive photomultiplier tube (PSPMT). Each scintillator matrix is made of 20×20 YAP:Ce finger crystal with dimensions $2 \times 2 \times 30$ mm^3. Each finger crystal is optically isolated with a 0.5 μm thick reflective layer from adjacent crystals and the same reflective coating is deposited on the back end, in order to collect all the light produced by a scintillation event toward the free end of the finger crystal which is coupled to the window of the PSPMT. The PSPMT has an intrinsic spatial resolution of about 0.5 mm for 2000 photon signals distributed on a 1 mm^2 surface (corresponding to a 511-keV energy deposit in YAP:Ce) and can recognize the position of the illuminated crystal.

The distance between two opposite detectors can be varied from 10 to 25 cm. With the detectors 15 cm apart both high spatial resolution (1.6-mm radial FWHM, 2.0-mm tangential FWHM, 1.8-mm axial FWHM) and high sensitivity (640 cps/μCi at center) can be achieved.

A. The Basic Concepts

A description of the actual YAP-(S)PET readout system can be found in [1]. The idea for the new electronics came from the fact that a time measurement was necessary together with a charge measurement. In fact the time difference between the dynode signals of the two detectors in a pair must be measured to allow optimal random coincidence noise rejection. YAP:Ce scintillator is very fast (27-ns decay) and the FWHM timing of a pair of detectors is 2 ns. Hardware coincideces with such narrow time windows are difficult to achieve. In the actual YAP-(S)PET readout system the time difference between paired PMTs is converted into a voltage value with an ORTEC time to amplitude converter (TAC) and registered, together with integrated anodic PSPMT signals, by a peak sensing analog to digital converter (ADC). Therefore, the design of a dedicated ADC board also implied the design of a time to amplitude converter (TAC) for the coincidence timing. Now the idea is completely different: we convert each charge signal into a digital pulse whose duration (time window) is proportional to the input charge. In this way, we measure all the time information, including the time difference between a pair of detectors, using a time to digital converted (TDC).

The main advantage of the new approach is the fact that digital instead of analog signals are transported from the readout

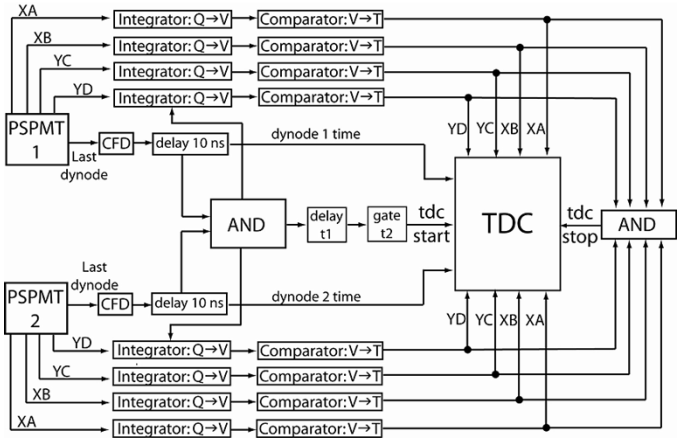

Fig. 1. Schematic diagram of the new YAP-(S)PET readout electronics.

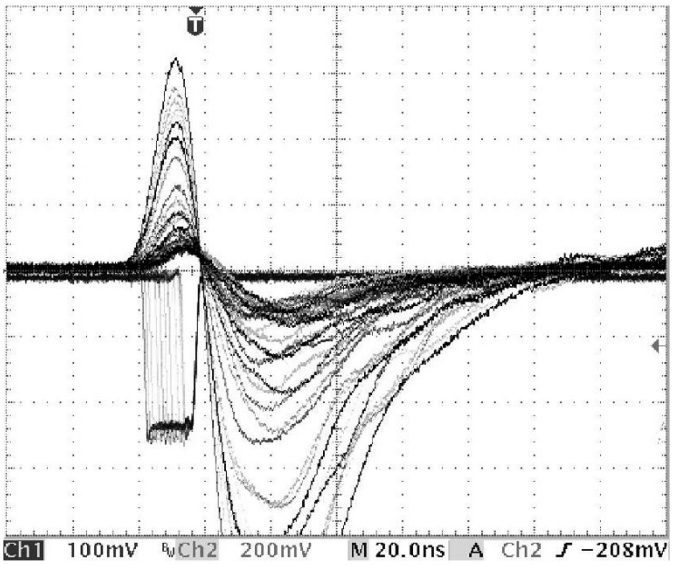

Fig. 2. Bipolar pulse obtained by the amplified and split last dynode output. Superimposed is the gate generated after the comparator. The rising (second) edge gives the start of the trigger logic.

electronics, which can be mounted directly on the scanner, to the acquisition system, placed a few meters away. The digital pulse-width coding technique would also allow the transmission of the charge information by means of rotating contacts which, by substituting the present coils of signal cables, would allow continuous rotation of the detector heads. The new electronics is also more compact and easy to transport than the standard CAMAC-NIM modular electronics used in the first prototype, which was suited for first performance studies, but is not the correct solution in a second phase of the prototype development where the electronics parameters are almost fixed and the imaging performances have to be investigated.

The schematic diagram of the new electronic readout is shown in Fig. 1 for one pair of detectors. Diagram details are explained in the following sections.

B. Dynode Signal Processing

The last dynode signals are use for trigger purposes. Each PMTs last dynode signal is sent to a first amplification stage and then to a constant fraction discriminator (CFD in Fig. 1) which generates a 10–15 ns long digital signal used to start acquisition. The amplifier and constant fraction discriminator are placed on a small home-made board placed very close to the photomultiplier tube (PMT) output to minimize the noise in the analog input signal.

The constant fraction discriminator working principle is the following. The last dynode output is inverted and amplified by a two-stage amplifier with a total gain of about 120 and then sent to a second processing stage in which the signal is split in two. The first of the two resulting signals is delayed by 10 ns; the second is inverted and attenuated by a factor 3. The two signals are then summed and a bipolar pulse is obtained which is sent to a comparator with a variable threshold. In this way, the output threshold is reached only if the input signal is greater than a fixed value and the position of the second edge of the comparator output is, therefore, fixed with respect to the starting time of the dynode signal, as can be seen in Fig. 2. The second edge of the comparator output signal has two uses. The first one is to give the synchronization time for the integration of the PMT anodic signals, the second one is to start a fixed length (15 ns) pulse which is used by the control logic to generate the trigger of the acquisition system. The constant fraction discriminator outputs are also sent as inputs to the TDC for coincidence time difference measurement (dynode 1 and dynode 2 time signals in Fig. 1).

C. Anodic Signal Processing

Hamamatsu R2486-06 amplification board is used in this first prototype to integrate and amplify the four PMT anodic signals. These four signals, XA, XB, YC, and YD are used to measure position and energy of the interaction point in the scintillator

$$X \propto \frac{(XA - XB)}{(XA + XB)} \tag{1}$$

$$Y \propto \frac{(YC - YD)}{(YC + YD)} \tag{2}$$

$$E \propto \frac{(XA + XB + YC + YD)}{4}. \tag{3}$$

Each of the four PMT outputs is integrated for a small time window (about 100 ns) over the signal peak, charging a 150-pF capacitor (integrator box in Fig. 1). At the end of the integration window the charged capacitor is discharge, with constant current, until a reference voltage level is reached (comparator box in Fig. 1). A time window is generated during the discharge whose length is proportional to the initial voltage across the capacitor and to the anodic signal amplitude (see Fig. 3). The four resulting time windows for each PSPMT are sent to a 32-channel time to digital converting system to be measured.

The anodic signal processing electronics is physically placed on a dedicated board, one for each PMT, connected by a 32 line interface to the board where the trigger control logic is performed. At the moment, the trigger control logic board is designed for a single pair of detectors, as explained in the next section, but the modularity of the system allows an easy upgrade to a scanner with more than one pair of opposite detectors, and eventually to a more complicated trigger logic.

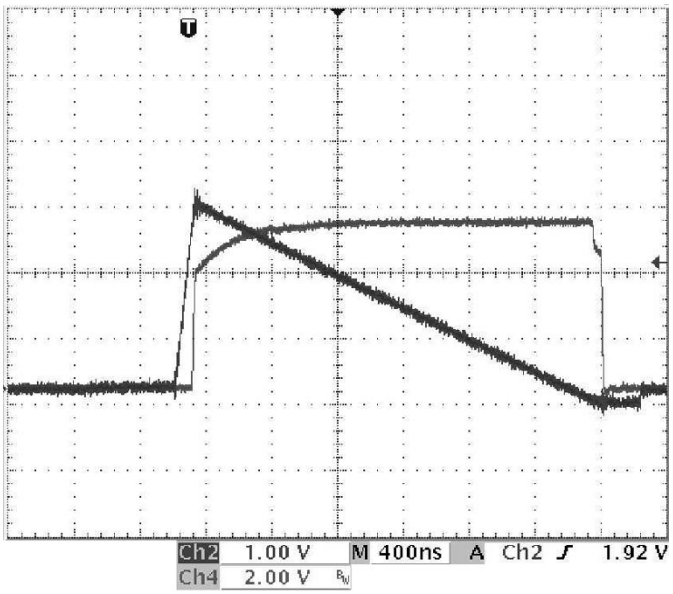

Fig. 3. Capacitor charge-discharge signal and time window generated during the constant current discharge phase. The length of the time window is proportional to the corresponding anodic signal amplitude. This time signal is sent to the time to digital converter.

D. Trigger Generation

The main component of the readout control logic is a programmable field programmable gate array (FPGA) which has several tasks. Its main function is to start the acquisition system once the correct logic requirements are achieved by the two 15-ns wide signals that come from the last dynode signal processing of the PMT pair. Trigger conditions can be chosen by changing a triple switch among the following possibilities:

1) coincidence (logical AND) of the dynode signals for PET trigger logic;
2) exclusive OR of the dynode signals for SPECT trigger logic;
3) first PMT signal alone for diagnostic purposes;
4) second PMT signal alone for diagnostic purposes;
5) coincidence between the first dynode signal and the second dynode signal, delayed by a fixed time for random coincidence noise evaluation;
6) external trigger signal for diagnostic purposes of the electronics without PMTs;
7) internal pulse generation for pedestal acquisition.

The TDC used in this version of readout electronics is capable of recording the occurrence of both the leading and the trailing edges of an input pulse (up to four transactions per input) with respect to a COMMON STOP signal, generated by the FPGA. The leading edge of the digital pulse encoding the charge information is common to all channels and it is in relation with the beginning of the discharge of the integrating capacitors, while the trailing edges are generated when the voltages of the individual integrating capacitors cross a common threshold level. The FPGA is in charge of generating the common STOP when all the anodic time windows are over. The FPGA also monitors the anode signals so that if the trailing edge of any of them is not detected within a programmable timeout interval (5 μs typical) the FPGA sets an error flag and resets all the readout electronics. The timeout value sets the maximum count rate achievable by the electronics and the dynamic range of the position and energy signals. The 5 μs value was chosen as a compromise between a high electronics rate and a correct energy range. The anodic signal discharge slope was tuned to use all the allowed 5 μs dynamic range.

Together with the eight anodic signals of the two PMTs other time signals are sent to the TDC. Last dynode, 15-ns wide, signals (dynode 1 and dynode 2 time signals in Fig. 1) allow the coincidence time difference measurement. If the delayed coincidence logic is allowed (trigger condition five) a time window is used to indicate that a delayed trigger condition was achieved. Finally, a time gate is generated if an error condition took place.

In this first set of measurements, we used a TDC chip developed by the K-long experiment (KLOE) collaboration for the acquisition system of the KLOE drift chamber [5]. The chip has 32 channels and a 6.4 μs dynamic range with 1-ns time resolution which is sufficient to guarantee the necessary energy and position resolution. In fact, the standard deviation for a constant anodic signal is 1.2 ns. The chip was mounted on a versa module Europe (VME) test board and a PowerPC 601 CPU on a Cetia VMTR2 board worked as master of the VME bus and controlled data acquisition.

III. New YAP-(S)PET Read Out Prototype Results

We tested the electronic prototype: in PET mode using a ^{22}Na point-like source between two detectors one equipped with a 5×5 crystal matrix and one with a 20×20 crystal matrix; in SPET mode using a ^{57}Co source and one detector with a 20×20 crystal matrix; finally, we made a series of rate studies using a ^{57}Co source and coupling a 30×30 crystal matrix to the window of a PSPMT.

A. PET Mode Tests

We used two detectors placed one in front of the other about 50 cm apart. One detector was equipped with a $4 \times 4 \times 3$ cm^3 YAP:Ce matrix (20×20 $2 \times 2 \times 30$ mm^3 finger crystals) and the second one with a $1 \times 1 \times 3$ cm^3 YAP:Ce matrix (5×5 $2 \times 2 \times 30$ mm^3 finger crystals). A point-like ^{22}Na source was placed at about 20 cm from the 5×5 matrix. The trigger to the acquisition system was given by the logical AND of the last dynode signals of the two PSPMTs.

The image of the 5×5 matrix as obtained on the PSPMT with this set-up is shown in Fig. 4. Each single $2 \times 2 \times 30$ mm^3 finger crystal can be clearly distinguished in the image. The energy spectrum of the same detector is shown in Fig. 5: the electronics threshold can be estimated at about 50 keV. The full width at half maximum (FWHM) energy resolution for the entire matrix is 25%.

The distribution of time differences between the signals from the two detectors is shown in Fig. 6. The time spectrum has a FWHM of 1.7 ns. The binning of the spectrum is limited by the TDC resolution (1 ns/channel).

B. Single Detector Acquisition Mode

We acquired a set of data with the electronics in single detector mode and a ^{57}Co source (122 keV). This test is impor-

Fig. 4. Image of the 5×5 crystal matrix directly coupled to the PSPMT with the electronics working in coincidence mode and a point-like ^{22}Na source placed between the two detector heads.

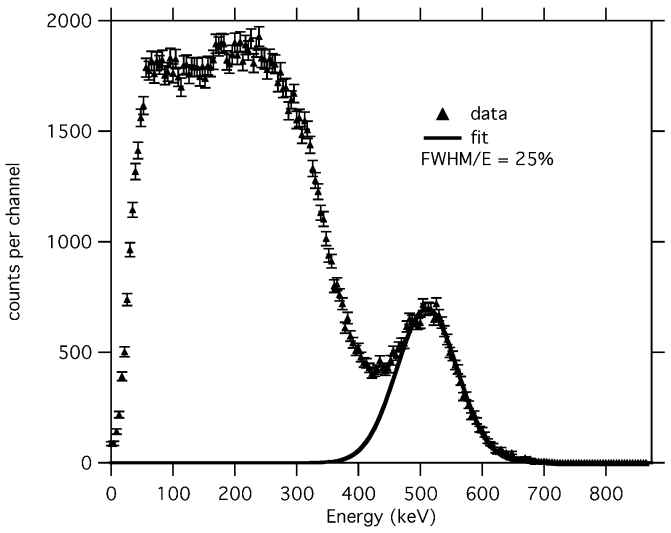

Fig. 5. Energy spectrum of 511-keV photons interacting in the 5×5 matrix obtained with the electronics working in coincidence mode and a ^{22}Na point-like source placed in between two PSPMTs. (X scale: 4.3 keV/ns).

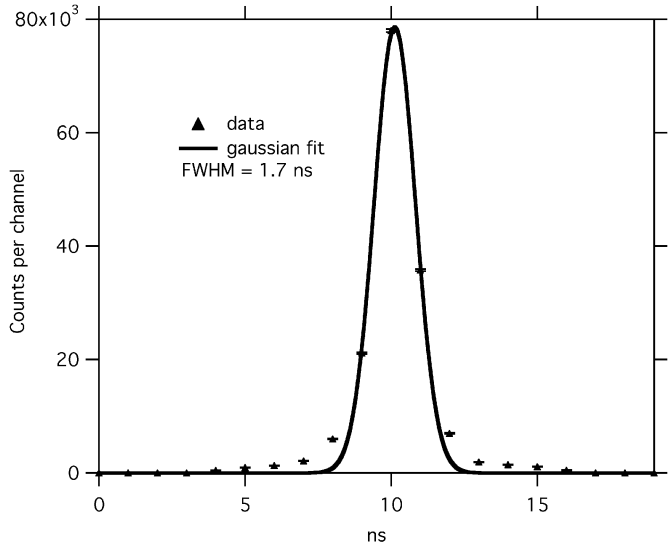

Fig. 6. Distribution of the time differences between the signals of the two detectors. The FWHM of the distribution is about 1.7 ns. The measurement was done with the electronics working in coincidence mode and a ^{22}Na point-like source placed between the two detector heads.

tant because it allows the investigation of the system performances at low energy and in SPECT mode. The 5×5 crystal matrix image obtained with this set-up is shown in Fig. 7. Each crystal can be clearly distinguished in the image. The spots appear slightly larger due to the fewer photoelectrons generated from 122 keV and 136 keV compared with 511-keV gammas. The pixels on the edges are more intense because the total flux of gamma rays is higher. In fact the crystal was not shielded and,

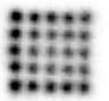

Fig. 7. Image of the 5×5 crystal matrix on the PSPMT obtained with the electronics working in single detector mode and using a ^{57}Co source.

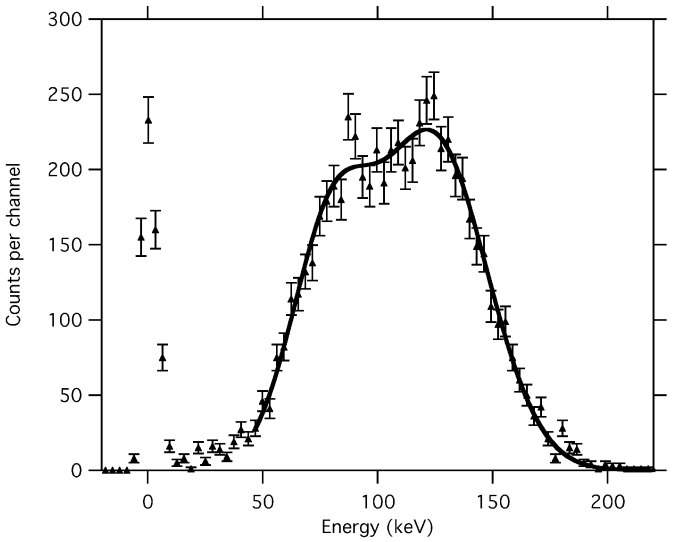

Fig. 8. Energy spectrum obtained with the electronics working in single detector mode and with a ^{57}Co source. Just events corresponding to a single crystal in Fig. 7 are added to the histogram. The spectrum is fitted with two gaussian functions: one describing 122-keV and 136-keV photo-peak events, the second one describing backscattering and lead K-flourence contamination. The energy resolution at 122 keV varies from 35% to 40% FWHM depending on the crystal element. (X scale: 3 keV/ns).

therefore, both scattered and lead K-fluorescence are incident of the edges whereas at the center of the matrix the elements are partly shielded.

The energy spectrum obtained selecting the events corresponding to a single crystal in the image in Fig. 7 is shown in Fig. 8.

The spectrum is fitted ($\chi^2 = 0.9$) with the sum of two gaussian functions, one describing the 122-keV and 136-keV photo-peak and the second one describing backscattering and K-flourence contamination due to the lead shielding surrounding the ^{57}Co source. The energy resolution varies from 35% to 40% FWHM at 122 keV depending on the crystal element. The peak due to electronic noise can be seen in the spectrum in Fig. 8 because the threshold of the electronic readout was set at a very low value (20 keV).

C. Rate Performance Study

We used a ^{57}Co source and the electronic readout in single detector acquisition mode to study the rate performance of the system. The detector was equipped with a $6 \times 6 \times 3$ cm^3 YAP:Ce crystal matrix (30×30 pixel crystals) which was slightly larger than the PSPMT photo-cathode window. We changed the system count rate varying the distance of the source from the detector.

The number of electronic triggers per second reached the maximum signal rate of the PSPMT (10^5 counts/s) when the source was placed next to the crystal. The acquisition rate is

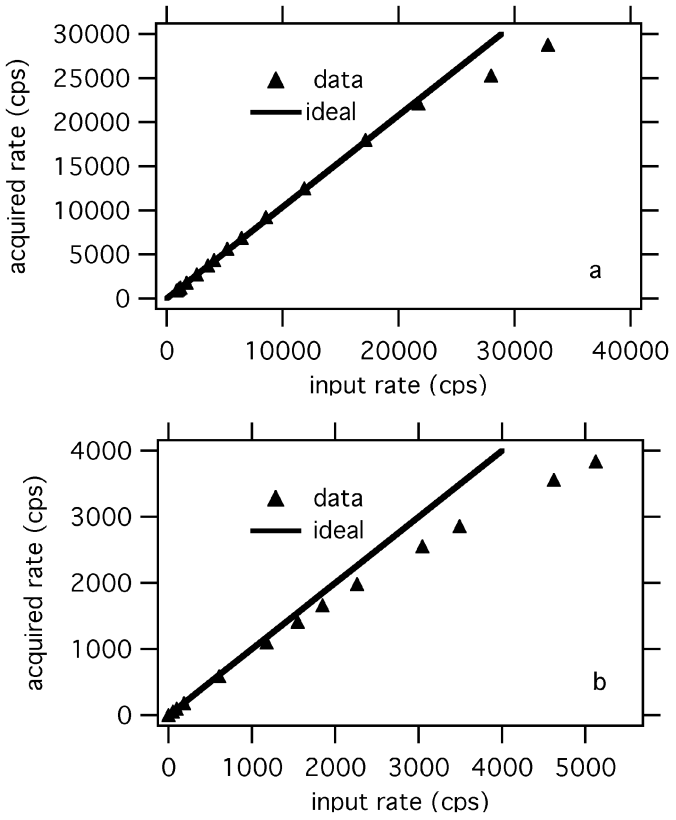

Fig. 9. (a) Number of events per second detected by the new acquisition system as a function of the number of triggers per second of the electronic readout. The straight line shows the ideal behavior. (b) Same curve for the NIM-CAMAC present system.

not linear with the number of electronic trigger per second. We measured the deviation from linearity of the acquisition rate as a function of electronic trigger rate by moving the source along the detector axis and recording the time spent by the acquisition program to record a fixed number of events. The electronic trigger rate was directly measured by giving the trigger signal as input to a standard NIM counter module. In Fig. 9(a) the number of events per second detected by the acquisition system (TDC and VME bus) as a function of the number of triggers per second of the electronic readout is shown. In Fig. 9(b), one can see the same curve for the NIM-CAMA system. The improvement is clear. The time spent to write data on disk is not included in these measurements. For the new electronics the behavior is linear up to 20 kHz and the saturation rate can be estimated at 30 kHz which is a much better value than the one obtained with the actual YAP–(S)PET electronics.

Our aim is to improve the rate performance of the system. At the moment the most critical point is the access to the TDC and to the VME bus, and could be improved with a better design of the TDC board and with the use of a faster CPU.

IV. Conclusion

The project for a new readout electronics for the YAP–(S)PET scanner and a complete set of tests on the first prototype were presented. The new readout satisfies the main compactness and modularity requirements and shows very good performances. Preliminary tests demonstrated the very good position and energy resolution capability of the detector equipped with the new electronics. The charge to time conversion used by the new readout does not affect energy or position measurement, and the energy resolutions obtained is the proper resolution. Time resolution is sufficient to reject noise due to random coincidences. The maximum count rate achievable is better than the one obtained with the present readout electronics, and further data acquisition system improvements are under study to further increase the count rate performances.

References

[1] A. Del Guerra, G. Di Domenico, M. Scandola, and G. Zavattini, "YAPPET: First results of a small animal positron emission tomograph based on YAP:Ce finger crystals," *IEEE Trans. Nucl. Sci.*, vol. 45, pp. 3105–3108, 1998.

[2] A. Del Guerra, C. Damiani, G. Di Domenico, M. Giganti, A. Motta, A. Piffanelli, L. Uccelli, G. Zavattini, V. Bettinardi, M. C. Gilardi, R. M. Moresco, and F. Fazio. (1999, Oct.) First in vivo studies on rats with the YAPPET scanner. *Conf. Rec. Nuclear Sci. Symp. Medical Imaging Conf.*

[3] A. Del Guerra, C. Damiani, G. Di Domenico, A. Motta, L. Sartori, and G. Zavattini, "An integrated PET-SPET small animal imager: Preliminary results," *IEEE Trans. Nucl. Sci.*, vol. 47, pp. 1537–1540, 2000.

[4] C. Damiani, A. Del Guerra, G. Di Domenico, M. Gambaccini, A. Motta, N. Sabba, and G. Zavattini, "An integrated PET-SPET imager for small animals," *Nucl. Instr. Meth.*, vol. A461, pp. 416–419, 2001.

[5] M. Passareo, E. Petrolo, and S. Veneziano, "A TDC integrated circuit for drift chamber read out," *Nucl. Instr. Meth.*, vol. A367, pp. 418–421, 1995.

[6] A. Del Guerra, F. De Notaristefani, G. di Domenico, R. Pani, and G. Zavattini, "Measurement of absolute light yield and determination of the lower limit for the light attenuation length for YAP:Ce crystal," *IEEE Trans. Nucl. Sci.*, vol. 44, pp. 2415–2418, 1997.